WELDING RESEARCH

SUPPLEMENT TO THE *WELDING JOURNAL*, JUNE 1988

Sponsored by the American Welding Society and the Welding Research Council

Rapid Solidification of Stainless Steels by Capacitor Discharge Welding

The effect of rapid solidification on the microstructure of stainless steel welds was examined

BY S. VENKATARAMAN AND J. H. DEVLETIAN

ABSTRACT. Capacitor discharge welding has been found to be a unique method to produce rapid solidification under the influence of an one-dimensional temperature gradient in welds up to 6.4 mm (0.25 in.) diameter. The objectives of this study were 1) to understand the role of process parameters in capacitor discharge welding to control the weld cooling rate during solidification, and 2) to apply the capacitor discharge process to study the microstructural modifications in austenitic stainless steels.

In the parametric study, arcing time and arc power density were the key factors controlling the cooling rate and thickness of the weld deposit. As a result, the capacitor discharge process parameters were developed to produce any desired cooling rate during solidification of stainless steels welds within the range from 10^6 to 6×10^7 K/s.

Microstructural modifications in rapidly solidified 304, 316 and 308 stainless steels were found to be dependent upon both cooling rate and Cr_{eq}/Ni_{eq} ratio. At cooling rates exceeding 10^6 K/s, Types 304 and 316 solidified entirely as primary austenite, while the Cr_{eq}-rich 308 solidified as primary ferrite in some grains and primary austenite in the remaining grains. The ratio of primary ferrite to primary austenite in the 308 weld increased with increasing Cr_{eq}/Ni_{eq} and decreasing cooling rate. The primary ferrite subsequently transformed to austenite by a massive transformation.

Capacitor discharge welding was shown to be an excellent method to study the rapid solidification of stainless steel welds.

S. VENKATARAMAN is a Metallurgist at the Indira Gandhi Centre for Atomic Research, Kalpakkam, India, and J. H. DEVLETIAN is a Professor in the Materials Science and Engineering Department, Oregon Graduate Center, Beaverton, Ore.

Based on a paper presented at the 67th Annual AWS Meeting, held April 13-18, 1986, in Atlanta, Ga.

KEY WORDS

Rapid Solidification
Stainless Steels
Capacitor Discharge
Discharge Welding
Stud Welding
Controlled Cooling
Austenitic Stainless
Arc Power Density
Arcing Time
Microstructure Change

Introduction

Although the capacitor discharge welding method has been commonly used for stud welding, it was first discovered to be a rapid solidification welding process as late as 1985 (Ref. 1). Prior to that time, the only recorded use of the capacitor discharge to produce rapidly solidified deposits was that of Jones (Ref. 2). In a subsequent heat flow modeling study, Einerson, *et al.* (Ref. 3), demonstrated that the weld deposit solidified under the influence of a unidirectional temperature gradient parallel to the stud axis. Thus, the modified capacitor discharge process was proven both experimentally (Ref. 4) and theoretically (Ref. 3) to be a one-dimensional heat flow welding process.

Joining of rapidly solidified crystalline materials without losing the metastable crystalline structures, grain refinement, reduced segregation, etc., for structural applications is a much desired goal. From this point of view, capacitor discharge welding is unique among joining pro-

Table 1—Chemical Compositions of Stainless Steels

Element	Grade 316	304	308
C	0.03	0.04	0.014
Mn	1.61	1.15	1.75
Si	0.52	0.38	0.75
Cr	17.86	17.48	19.67
Ni	12.55	9.36	10.21
Mo	2.85	0.19	0.17
Cu	0.10	0.24	0.067
S	0.010	0.022	0.006
P	0.023	0.030	0.022
N	0.094	0.04	0.052

cesses in that it is the only one capable of producing joints up to 6.4 mm in diameter at cooling rates greater than 10^6 K/s (Refs. 1, 4). In comparison, laser and electron beam welds having the same cooling rate as capacitor discharge welding are so small that actual fused joints between two structural components are not practical.

Structures produced in stainless steels during conventional welding conditions for varying compositions and cooling rates have been extensively studied and characterized (Refs. 5–10). By contrast, many interesting phenomena occurring during rapid solidification processing of these materials have not been fully explainable (Ref. 11). Application of rapid solidification to austenitic stainless steels has been found to suppress ferrite formation (Refs. 1, 11) and to reduce hot cracking during laser beam welding (Ref. 11). The technical importance of rapid solidification during welding of stainless steels is, therefore, clear.

The objectives of the following study were, therefore, to 1) gain an understanding of the role of the significant process parameters in capacitor discharge welding to control and predict the weld cooling rate during solidification, 2) optimize capacitor discharge welding to produce the most rapid cooling rates while maintaining structurally sound welds, and 3) investigate microstructural modifications produced by capacitor discharge welding of stainless steels.

Table 2—Chromium and Nickel Equivalents and Predicted Solidification Modes for Stainless Steel Welds by GTAW

Stainless steel grade	316	304	308
DeLong equivalents			
Cr_{eq}	21.49	18.24	21.00
Ni_{eq}	17.08	12.48	13.22
Cr_{eq}/Ni_{eq}	1.26	1.46	1.59
Predicted FN	2	2	10
Actual FN	2–3	2–4	9–10
Hammar-Svensson equivalents			
Cr_{eq}	22.54	18.31	21.06
Ni_{eq}	15.14	11.48	11.94
Cr_{eq}/Ni_{eq}	1.49	1.59	1.76
Predicted solidification mode	AF[a]	FA[b]	FA–F[c]

(a) AF – Primary austenite-ferrite.
(b) FA – Primary ferrite-austenite.
(c) F – Primary ferrite.

Procedure

Materials

The compositions of 304, 308 and 316 stainless steels used in the present study are shown in Table 1. Gas tungsten arc welds were made in all three types and observed for ferrite contents and solidification mode for comparison with capacitor discharge weld metal. Chromium and nickel equivalents were calculated by two different methods. Observed ferrite contents were closely predicted by the DeLong method (Ref. 12), and solidification mode was predicted by the Hammar and Svensson method (Ref. 8), as shown in Table 2. The approximate positions of the three alloys on the 70% Fe vertical section of the Fe-Cr-Ni equilibrium diagram is shown in Fig. 1.

Stud Preparation

Welds were made between cylindrical studs. Alloy 304 was available as 6.4-mm-diameter rod and 316 as 16-mm (0.63-in.) thick plate, from which rods of the required diameter were machined. Alloy 308 was machined from undiluted weld metal deposited by GTAW. The as-deposited 308 alloy, which contained an FN of 10, was then homogenized at 1100°C (2012°F) for 12 h before capacitor discharge welding. The FN after homogenization dropped to 2. Conical ignition tips were machined onto one of the two studs making the joint.

Equipment and Welding Procedure

The setup of components joined by initial gap capacitor discharge welding is shown in Fig. 2. The studs impact under gravity, causing arcing and subsequent melting by discharge of a capacitor bank. As the components meet, the arc is extinguished, solidification occurs, and excess liquid is expelled to produce the joint. Descriptions of the process are also available in the literature (Refs. 13, 14). The principal variables considered were drop height, stud diameter, ignition tip length, drop weight, capacitance and voltage, as shown in Fig. 2. The welding conditions used are shown in Table 3. The components were weighed before and after welding to an accuracy of 10^{-4} g in order to measure weight of metal expelled during welding. Current, voltage and stud acceleration profiles were mea-

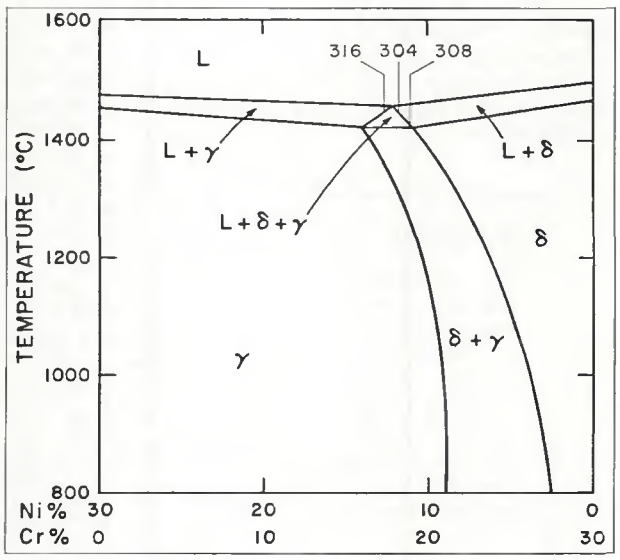

Fig. 1—Approximate compositions of stainless steels superimposed on the vertical section of the Fe-Cr-Ni phase diagram at 70% Fe

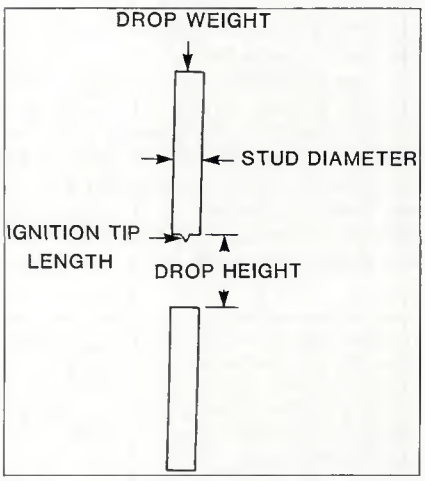

Fig. 2—Setup of components to be welded by the capacitor discharge process showing process variables

sured during welding by using a digital storage oscilloscope.

Microscopy

Capacitor discharge welds were sectioned transverse to the weld for metallographic preparation. After conventional rough polishing, specimens were electropolished for 10 to 15 s in 330-ml water, 550-ml phosphoric acid, and 120-ml sulphuric acid solution. Polishing occurred at 20 to 25 V, and etching was accomplished using the same solution at 1.5 to 2 V for 60 s. Specimens were then observed optically.

Transmission electron microscopy was performed on 304 stainless steel capacitor discharge welds. Foils of weld metal were sectioned and mechanically thinned to 100 μm before final electrolytic thinning in 30% nitric acid in methanol at 0°C (32°F) and 15 V.

Measurement of Interdendritic Spacing

Primary and secondary dendrite arm spacings were measured by an intercept method and average values were used to estimate cooling rates. Average dendrite spacings were within 10% of the mean. Cooling rates during solidification were estimated using the Grant relationship (Ref. 15) for secondary dendrite arm spacings in splat-quenched stainless steels. The values for capacitor discharge welding ranged between 10^6 and 6×10^7 K/s, as seen in Fig. 3.

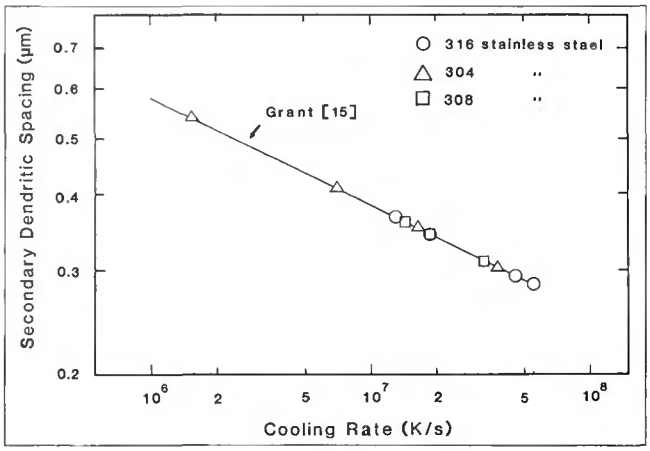

Fig. 3 — Cooling rates calculated from Grant's relationship (Ref. 15) using secondary dendrite arm spacings measured in stainless steel capacitor discharge welds

Results

Process Control and Optimization

Since no prior information was available on the effects of capacitor discharge welding variables on significant weld metal characteristics, a parametric study was conducted to produce controlled cooling rates, while still maintaining full fusion in the weld. Reducing weld thickness was taken as the significant factor in producing fast cooling rates during welding, since reduced dimensions along the heat flow direction (in this case, the thickness direction) have been shown to promote rapid solidification (Ref. 15).

Welds were made in 6.4-mm-diameter stainless steel by varying drop height, ignition tip length, voltage and drop weight at two levels, and average weld thickness was measured in each case. As Figs. 4 and 5 show, weld thickness decreased with increasing drop height and decreasing ignition tip length. A reduction in voltage also decreased weld thickness, while drop weight did not have a significant effect. However, a voltage of 90 was found to be optimum for good fusion. Therefore, ignition tip length and drop height were identified as the most significant variables in producing rapid solidification.

As a result of the parametric study of the process, weld conditions were selected to provide a wide range of cooling rates during solidification. For convenience, three sets of parameters shown

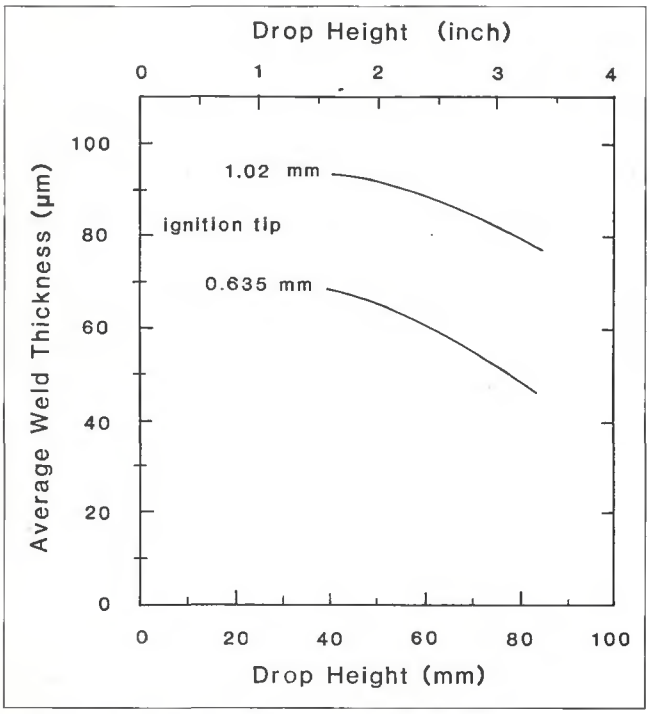

Fig. 4 — Average weld thickness as a function of drop height and ignition tip length during capacitor discharge welding

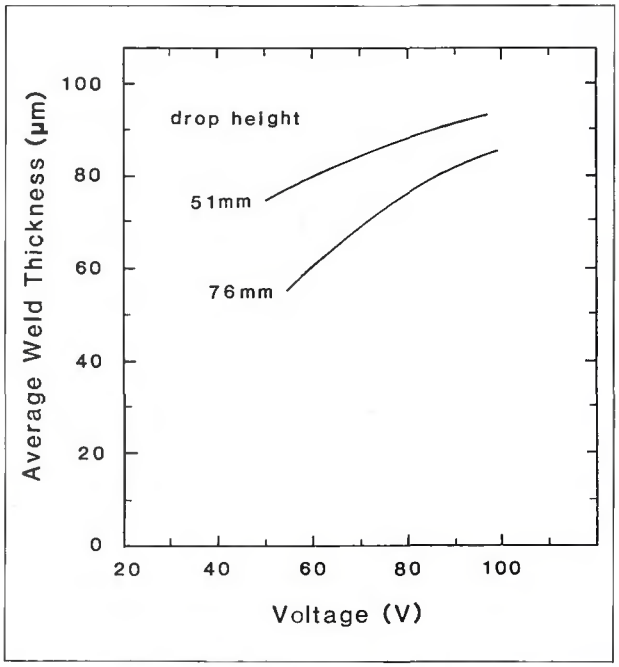

Fig. 5 — Average weld thickness as a function of voltage for different drop heights during capacitor discharge welding

in Table 3 were designated to produce "slow," "intermediate" and "fast" cooling welds. This terminology will be used in referring to weld microstructures. The current and voltage profiles measured during welding showed that arc times varied from 0.3 to 0.5 and 1 ms for fast, intermediate and slow cooling conditions, respectively—Figs. 6A to C. The corresponding cooling rates are shown below:

Weld:	Slow	Intermediate	Fast
Cooling rate, K/s:	10^6	2×10^7	6×10^7

A reduction in arc time produced a decrease in weld thickness, and average weld thickness increased linearly with square root of arc time, as in Fig. 7. The total quantity of molten metal decreased with decreasing arc time, and in Fig. 8, it is also seen that the total amount of molten metal was much greater than that present in the weld, due to expulsion as spatter.

Thus, process variables were found to substantially affect cooling rate during solidification. An equation for the arc power density (P) in capacitor discharge welding was developed to quantitatively describe the effects of process variables on cooling rate during welding:

$$P = \frac{CV^2}{4at}$$

where t = arc time, C = capacitance, V = voltage, and a = stud cross-sectional area.

Raising the power density increased the cooling rate during solidification in capacitor discharge welding, while reducing the dendrite arm spacing of the weld metal, as shown in Fig. 9.

Table 3—Designations and Welding Conditions Used for Microstructural and Process Study of Capacitor Discharge Welding of Stainless Steels

Weld Designation and No.	Diameter (mm)	Capacitance (mF)	Voltage (V)	Drop Height (mm)	Drop Weight (N)	Ignition Tip Length (mm)
1. Slow A1[(a)] to C1[(c)]	6.4	80	90	51	60	1.01
2. Intermediate A2 to C2	6.4	80	90	76	78	0.64
3. Fast A3 to C3	3.2	40	90	76	41	0.32
4. A4	3.2	40	90	76	22	0.09
5. A5	2	8	150	76	22	0.75
6. B6[(b)]	6.4	80	90	51	60	2.03
7. B7	6.4	80	90	51	60	1.52

(a) A – 316 Stainless steel
(b) B – 304 Stainless steel
(c) C – 308 Stainless steel

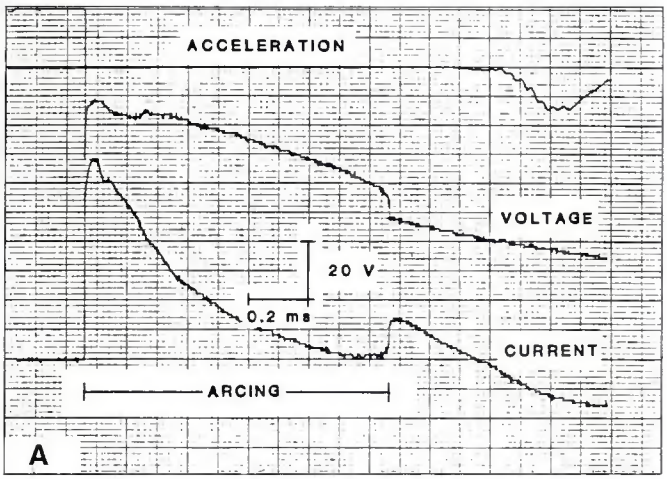

Fig. 6 – Typical current, voltage and stud acceleration profiles of capacitor discharge welds made under: A – "slow;" B – "intermediate;" C – "fast" cooling conditions

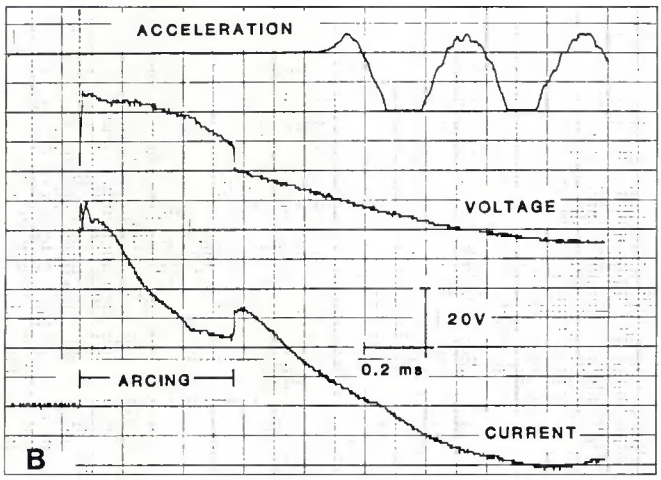

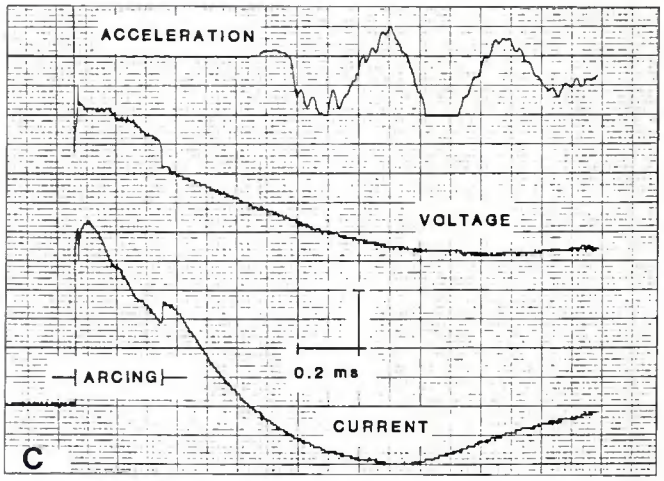

Microstructural Modification by Capacitor Discharge Welding

Capacitor discharge weld metal exhibited fully austenitic microstructures for 304, 316 and 308 stainless steels. The fully austenitic structure in the fusion zone was verified by careful optical microscopic observation under different etching conditions. The microstructures of 304 stainless steel weld metal deposited by capacitor discharge welding were fully austenitic and solidified as cells or cellular dendrites, as shown in Figs. 10A to C. The refinement in dendritic structure with weld parameters is apparent from slow to fast cooling conditions. By comparison, the very slow cooling weld metal deposited by the GTAW process showed an FN of 2 to 3, as seen in Fig. 11. Previous work (Refs. 1, 4) on 304 stainless steel demonstrated the reduction in ferrite content with increasing solidification rate up to about 10^6 K/s, beyond which only austenitic structures solidified. Alloy 316 showed microstructures similar to those

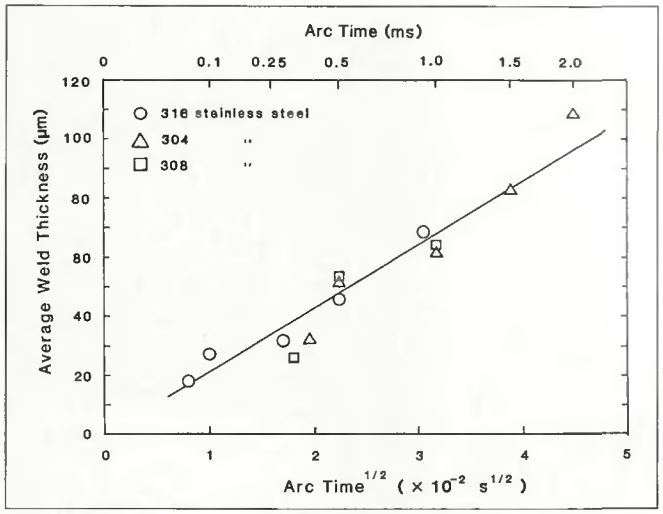

Fig. 7 — Average weld thickness as a function of arc time in capacitor discharge welding

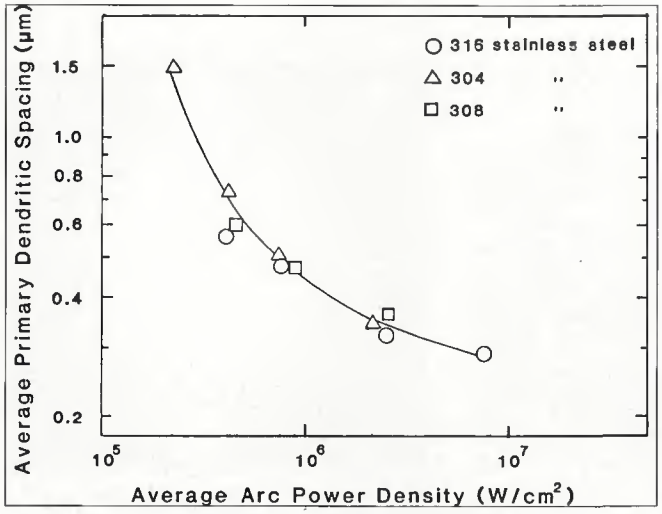

Fig. 9 — Primary dendritic spacings in stainless steel as a function of arc power density during capacitor discharge welding

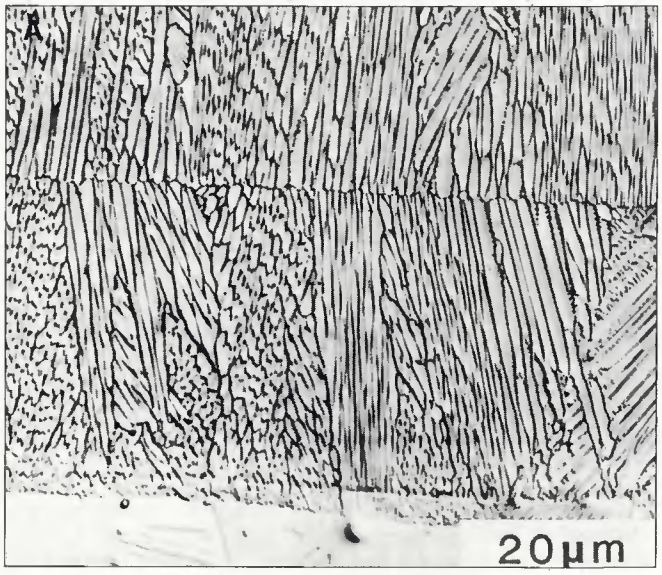

Fig. 10 — Dendritic structures of capacitor discharge welds in 304 stainless steel. A — Slow cooling conditions; B — intermediate cooling conditions; C — fast cooling conditions

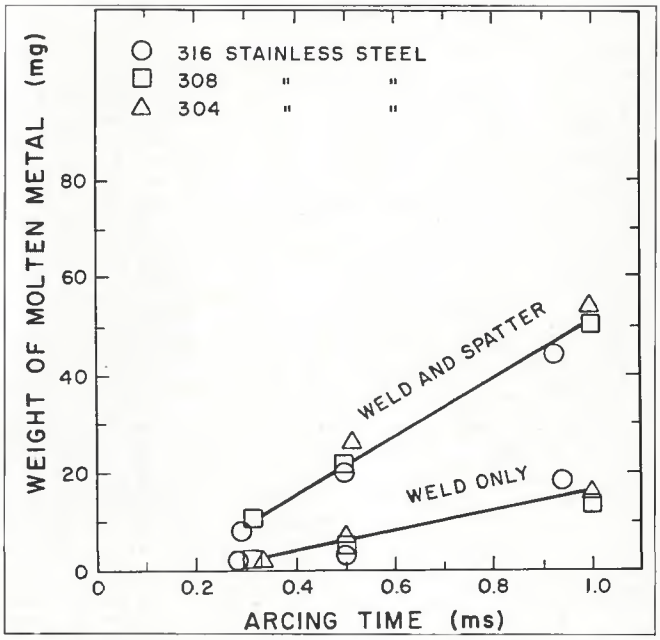

Fig. 8 — Weight of molten metal in the weld, and including spatter, as a function of arc time

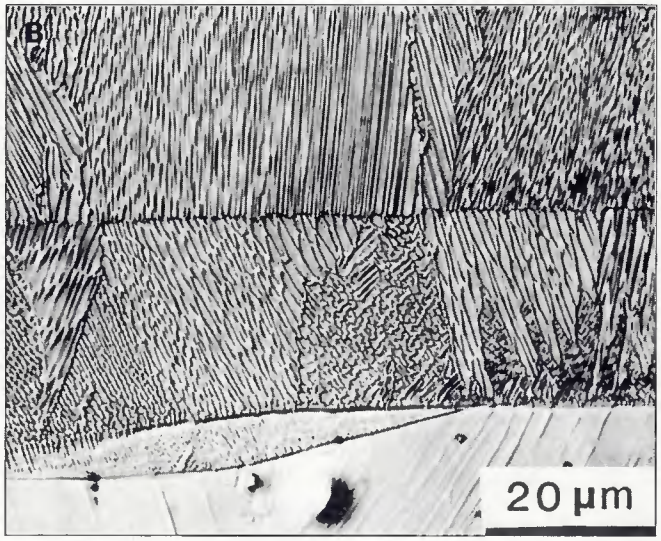

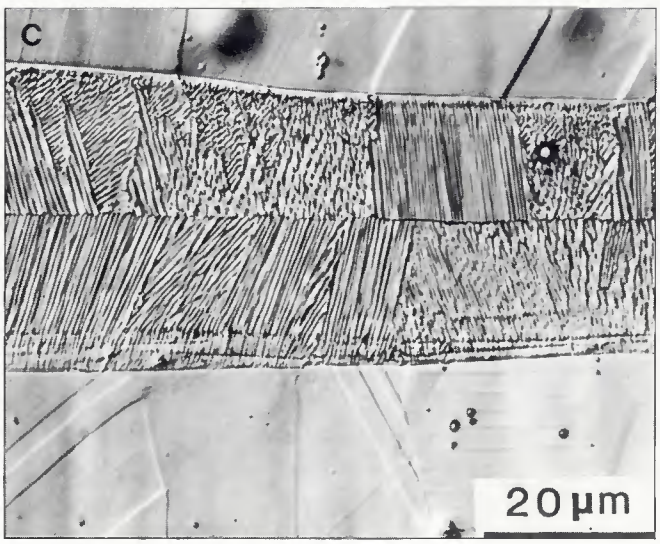

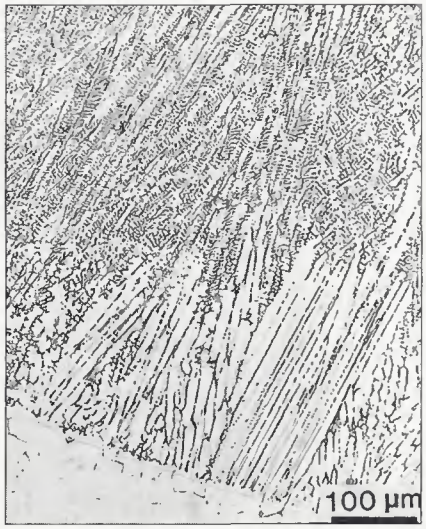

Fig. 11 — Dendritic structure of gas tungsten arc weld in 316 stainless steel showing ferrite morphologies

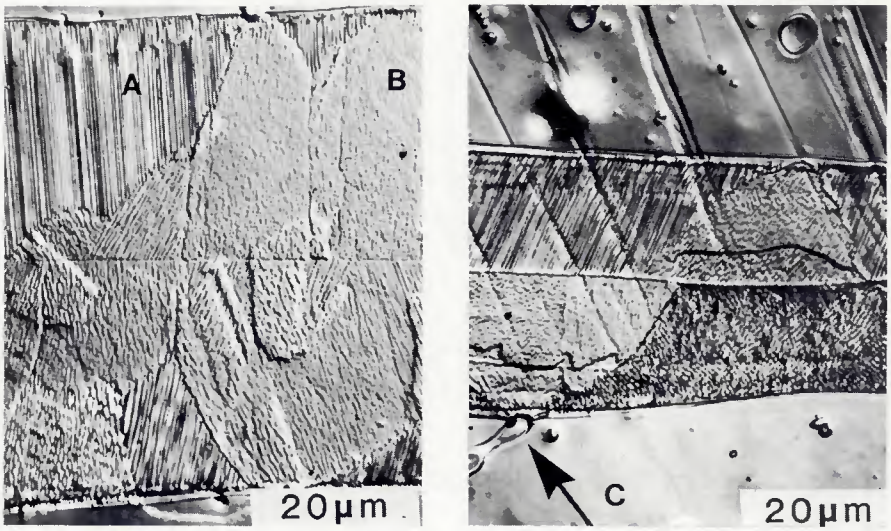

Fig. 13 — Dendritic structures of capacitor discharge welds in 308 stainless steel under (left) slow cooling conditions and (right) fast cooling conditions. Letters show ferrite in contact with the fusion zone: A — primary austenite; B — primary ferrite; C — ferrite

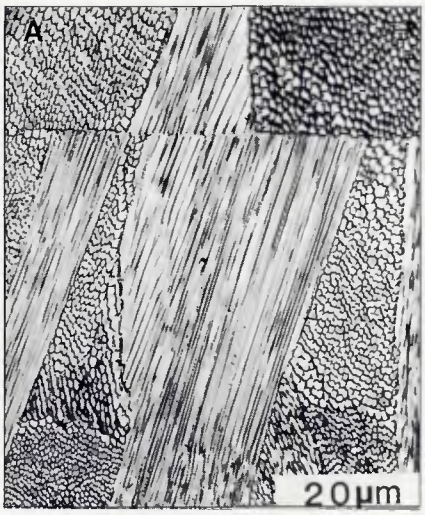

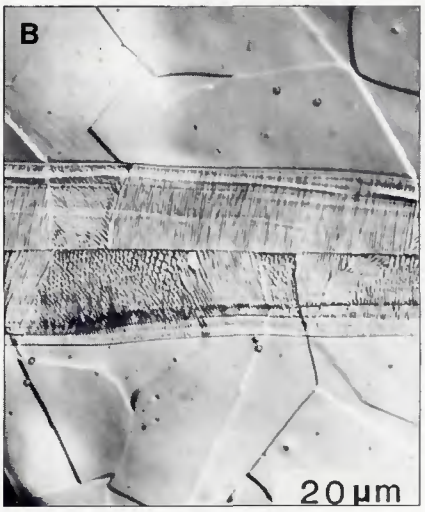

Fig. 12 — Dendritic structures of capacitor discharge welds in 316 stainless steel. A — Slow cooling conditions; B — fast cooling conditions

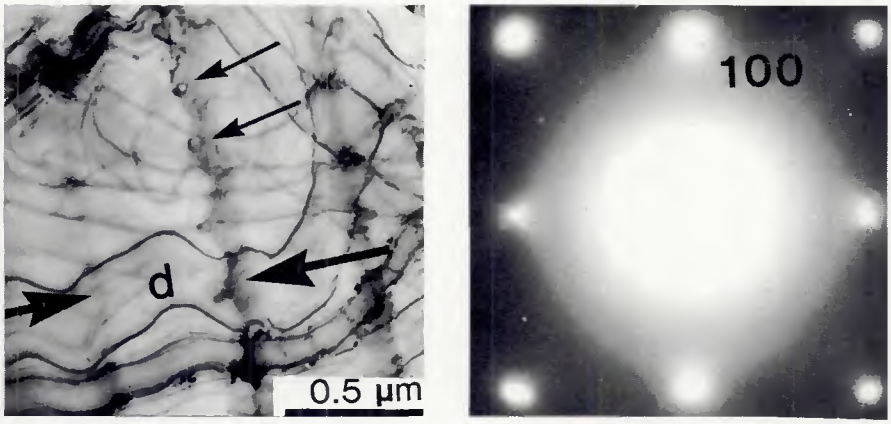

Fig. 14 — Transmission electron microscopy of slow cooling capacitor discharge weld in 304 stainless steel: (left) bright field image; (right) diffraction pattern. Arrows point to vacancy dislocation loops. The cell width "d" is also indicated

in 304 capacitor discharge weld metal — Fig. 12.

The 308 stainless steel capacitor discharge weld metal showed fully austenitic structures in the fusion zone, as seen in Fig. 13. However, because a small amount of ferrite was present in 308 base metal, primary ferritic solidification occurred by epitaxial growth, as indicated by the arrow in Fig. 13B. The ferrite "islands" extended beyond the fusion line into the fusion zone, due to ferrite's higher melting temperature relative to the austenite. During solidification, the primary ferritic regions expanded from the base metal ferrite to dominate the microstructure and were characterized by recrystallization across epitaxial grain boundaries and dendrites. The recrystallization was identified as due to the solid-state transformation from primary ferrite to austenite during cooling. Also, the primary austenitic regions were pinched off by expanding primary ferrite regions, indicating faster growth for the latter or more preferred orientation. The portions of the 308 welds that solidified as primary austenite exhibited clearly defined cells and cellular dendrites. However, those regions that were primary ferritic were diffuse and poorly defined, as illustrated in Fig. 13. The diffuseness of the ferritic substructure was due to the substantially reduced segregation ratio caused by a two orders of magnitude difference in diffusion coefficient of alloying elements in ferrite compared to austenite (Ref. 6).

Transmission Electron Microscopy

Transmission electron microscopy of 304 stainless steel weld metal deposited by capacitor discharge welding under slow cooling conditions revealed cell/dendrite boundaries to be decorated by a high dislocation density, and the formation of vacancy dislocation loops, seen in Figs. 14 and 15. In Fig. 14, the vacancy dislocation loops are indicated by arrows.

The dendrite growth direction was of the <100> type, as seen from Fig. 14. No second phase could be identified, confirming the fully austenitic structure.

Discussion

Controlling Cooling Rates during Capacitor Discharge Welding

Ignition tip length and drop height were found to be the most effective parameters to control the arc time required to consume the ignition tip. Arc time was the single most significant factor controlling weld cooling rate through its effects on weld thickness and the power density equation. The strong dependence of the weld thickness on arc time despite different heat inputs could be related to the fact that the most superheated liquid was the most likely to be expelled from the weld pool during impact of the faying surfaces. The cooling rate in the weld metal increased with decreasing arc time by increasing the power density—Fig. 9. Therefore, arc time was identified as the most important variable to produce and control cooling rates during rapid solidification.

The relationship between weld thickness and square root of solidification time is well known in castings and ingots (Ref. 16), and also in laser surface melting (Ref. 17). This dependence of weld thickness and cooling rate on arcing time and power density is also observed in the capacitor discharge process under one dimensional heat flow conditions. Similarly, in laser beam welding, an increase in absorbed power density has been shown to increase cooling rate (Refs. 17, 18).

Cooling rates attained during capacitor discharge welding ranged from 10^6 to 6×10^7 K/s. The process is, therefore, unique in its capability to join large diameters (6.4 mm) compared to other rapid solidification welding processes, such as laser and electron beam welding. For example, a laser beam weld which has solidified at a cooling rate of 10^7 K/s would be so small (Ref. 17) that only surface melting (and not welding) would be achieved. The present study provides a means to obtain such cooling rates with capacitor discharge welding in a controlled manner under one-dimensional heat flow conditions. The sections joined are so large that tensile testing can even be performed on the rapidly solidified weld joint.

Microstructural Modifications—Solidification Phenomena

The compositions of the three alloys studied are shown on the vertical section of the Fe-Cr-Ni phase diagram in Fig. 1. Alloys 304 and 308 fall on the primary ferritic side of the eutectic point, while 316 is very close to the eutectic point on the primary austenitic side. Gas tungsten arc weld microstructures confirmed solidification modes predicted by Suutala (Ref. 7). As seen in Table 2, ferrite was present in all three materials in weld metal deposited by autogenous GTAW. By contrast, the solidification mode was entirely austenitic in 304 and 316 stainless steel capacitor discharge welds—Figs. 10 and 12. These fully austenitic structures produced by rapid solidification are in general agreement with the work of David, *et al.* (Ref. 23).

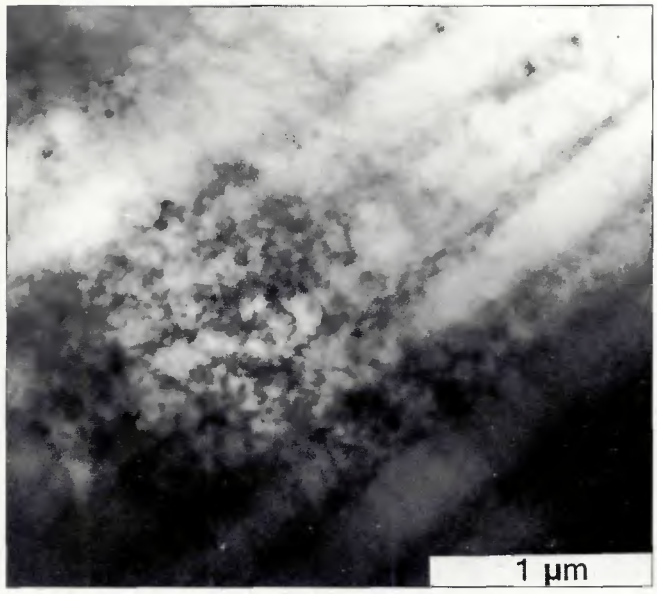

Fig. 15—Transmission electron micrograph of slow cooling capacitor discharge weld in 304 stainless steel

The 308 alloy exhibited a mixed solidification mode where some grains solidified as ferrite, while others solidified as austenite. The rapid epitaxial growth of primary ferrite in 308 indicated that the absence of a substrate for ferrite growth resulted in a fully austenitic solidification structure in 304 and 316 stainless steels. Thus, full epitaxial growth in all capacitor discharge weld microstructures occurred to the exclusion of nucleation and growth of the second phase—in this case, ferrite. That this occurred to a limited extent even in GTA weld metal is apparent from Fig. 11, where epitaxial growth close to the base metal took place as primary austenite (and interdendritic ferrite), while further into the fusion zone primary ferrite has formed.

By virtue of its greater Cr_{eq}/Ni_{eq} ratio, the 308 alloy exhibited a mixed solidification mode, where some grains solidified epitaxially as primary ferrite, while others solidified as primary austenite, as illustrated in Fig. 13A. With increasing cooling rate from 10^6 to 6×10^7 K/s, the 308 alloy weld metal tended to solidify with greater proportions of primary austenite. Apparently, microstructural modifications involving primary austenitic solidification in alloys that normally solidify as delta ferrite are facilitated by decreasing Cr_{eq}/Ni_{eq} ratios. Also, the critical solidification rate required to produce such microstructural modifications must be greater for the high Cr_{eq}/Ni_{eq} ratio alloys (308 alloy) and substantially less when the ratio is low (304 and 316 alloys).

Transmission electron microscopy revealed vacancy dislocation loops in the intercellular regions similar to those observed by Wood and Honeycombe (Ref. 19) in splat-quenched austenitic stainless steel, which confirmed the effect of high crystal growth rates on defect structure. The presence of aligned dislocations parallel to the cell axis combined with vacancy loops is characteristic of rapid solidification structures (Ref. 20).

Solid-State Transformation

The fully austenitic structures observed in 308 stainless steel capacitor discharge weld metal, while both primary ferritic and austenitic solidification occurred, indicated that a solid-state transformation had occurred from ferrite to austenite. This transformation in stainless steel weld metal has been shown to occur by a diffusional mechanism under GTA weld cooling conditions by several investigators (Refs. 6, 9). The massive mechanism for the same transformation has also been proposed (Ref. 21).

The diffusional transformation should occur by growth of Widmanstatten plates of austenite into the delta ferrite. At high cooling rates, this reaction would not go to completion, due to limited time available for solute diffusion. In the present case, the transformed regions were fully austenitic. No fine structure was observable under the highest optical

magnifications, and therefore, there was no evidence of a diffusional transformation.

On the other hand, the occurrence of recrystallization during transformation is only possible by a sweeping incoherent transformation interface, which is unique to the massive type of transformation (Ref. 22). The fully austenitic structure of the transformed regions and the absence of any evidence of incomplete diffusional growth show that the massive transformation should have occurred. Thus, while the thermodynamic favorability for the massive transformation in stainless steels has been recognized previously in the literature, favorable kinetic conditions for the transformation—namely, sufficiently high cooling rates and epitaxial growth—could be achieved under capacitor discharge welding conditions.

Conclusions

The following conclusions ensued from the study of rapid solidification of stainless steels by capacitor discharge welding:

1) Arc time was the most significant variable in producing controlled cooling rates during solidification. Decreasing arc time resulted in increased weld cooling rates up to a maximum estimated value of 6×10^7 K/s. The slowest cooling rate achievable was approximately 10^6 K/s.

2) Solidification of 304 and 316 stainless steels was primary austenitic. Epitaxial growth from the fully austenitic substrate into the melt resulted in the exclusion of the normal solidification of ferrite.

3) Mixed mode solidification of primary ferrite and primary austenite occurred in 308 stainless steel weld fusion zone. Primary ferrite subsequently transformed to austenite during rapid cooling, possibly by a massive transformation.

4) The cooling rate required to achieve full primary austenitic solidification increased with increasing Cr_{eq}/Ni_{eq} ratio of the alloy.

5) Capacitor discharge welding is the only process capable of producing joints of large cross-sectional area under rapid solidification and one-dimensional heat flow conditions.

Acknowledgments

The authors wish to thank the Welding Research Council and the Oregon Graduate Center for supporting this work. Special thanks are also in order to Sin-Jang Chen for his helpful advice and assistance in metallography.

References

1. Devletian, J. H., and Wood, W. E. 1985. Paper presented at the *66th Annual AWS Convention*, Las Vegas, Nev.
2. Jones, H. 1969. *Mat. Sci. Eng.* 5(1):1–18.
3. Einerson, C. J., Clark, D. E., and Devletian, J. H. 1987. To be published in the *Proceedings of 2nd ASME/JSME Thermal Engineering Joint Conference on Heat Transfer in Manufacturing and Materials Processing*, Hawaii.
4. Venkataraman, S. 1986. *Rapid Solidification of Stainless Steels and FeAl Ordered Alloy by Capacitor Discharge Welding.* M. S. Thesis. Oregon Graduate Center, Beaverton, Ore.
5. Katayama, S., Fujimoto, T., and Matsunawa, A. 1985. *Trans. JWRI* 14(1):123–138.
6. Boothby, R. M. 1986. *Mat. Sci. Tech.* 2(1):78–87.
7. Suutala, N., and Moisio, T. 1983. *Solidification Technology in the Foundry and Cast House*, pp. 310–314, The Metals Society, London, England.
8. Hammar, O., and Svenson, U. 1979. *Solidification and Casting of Metals.* The Metals Society, London, England, pp. 401–410.
9. Brooks, J. A., Williams, J. C., and Thompson, A. W. 1982. *Trends in Welding Research in the United States*, ed. S. A. David, pp. 331–357, ASM International, Metals Park, Ohio.
10. Takalo, T., Suutala, N., and Moisio, T. 1979. *Met. Trans.* 10A:1173–1181.
11. Vitek, J. M., and David, S. A. 1983. *Met. Trans.* 14A:1833–1841.
12. DeLong, W. T. 1974. *Welding Journal* 53:273-s to 286-s.
13. Cubberly, W. H., *et al.* 1983. *Metals Handbook, Ninth Edition*, Vol. 6:739–740, ASM International, Metals Park, Ohio.
14. Kearns, W. H., ed. 1978. *Welding Handbook*, Seventh Edition, Vol. 2: 282–294. American Welding Society, Miami, Fla.
15. Grant, N. J. 1983. *J. of Metals* 35(1):20–27.
16. Flemings, M. C. 1974. *Solidification Processing.* McGraw-Hill, New York, N.Y., p. 364.
17. Greenwald, L. E., Breinan, E. M., and Kear, B. H. 1979. *Laser-Solid Interations and Laser Processing*, eds. S. D. Ferris, *et al.*, p. 189, American Institute of Physics.
18. Hsu, S. C., Chakravorty, S., and Mehrabian, R. 1978. *Met. Trans.* 9B:221.
19. Wood, J. V., and Honeycombe, R. W. K. 1976. *Mat. Sci. Eng.* 23:107–112.
20. Nishi, Y., Tachi, M., and Yajima, E. 1985. *Scripta Met.* 19:865–866.
21. Lippold, J. C., and Savage, W. F. 1984. *Welding Journal* 60:362-s to 374-s.
22. Perepezko, J. H. 1984. *Met. Trans.* 15A:437–447.
23. David, S. A., Vitek, J. M., and Hebble, T. L. 1987. *Welding Journal* 6(10):289-s to 300-s.